State of the Art in Interventional Oncology: Case Discussions

Case-based discussions highlighting the use of interventional oncologic treatments for hepatocellular carcinoma, renal cell carcinoma, biliary stricture due to malignancy, and palliative pain management.

With Mohammad Bader, MD; Suvranu Ganguli, MD, FSIR; Paraag R. Gupta, BS; Amy R. Deipolyi, MD, PhD, FSIR; Christopher R. Bailey, MD; Kelvin Hong, MD; Raul N. Uppot, MD, FSIR, FSAR; and Reiner Henson B. See, MD

Radiation Segmentectomy for Hepatocellular Carcinoma in the Setting of Celiac Artery Occlusion

By Mohammad Bader, MD, and Suvranu Ganguli, MD, FSIR

CASE PRESENTATION

A man in his early 60s with HIV, hypertension, coronary artery disease, peripheral artery occlusive disease, and well-compensated Child-Pugh A hepatitis C cirrhosis was incidentally found to have a liver mass during workup of microhematuria. CT and subsequent MRI showed an arterially enhancing, 5.6-cm mass with washout on delayed-phase imaging, consistent with a Liver Imaging Reporting and Data System (LI-RADS) 5 lesion (definite hepatocellular carcinoma [HCC], Figure 1). Due to his comorbidities, the patient was not deemed a surgical candidate, and given the size of the tumor, thermal ablation was not felt to be optimal. After multidisciplinary tumor board discussion, the patient was referred for yttrium-90 (Y-90) radiation segmentectomy.

PROCEDURAL OVERVIEW

Review of the preprocedural imaging showed celiac artery occlusion, likely from a combination of compression by the median arcuate ligament as well as atherosclerotic disease (Figure 2). Mapping angiography was also notable for a celiac origin occlusion, which could not be traversed. Superior mesenteric artery (SMA) arteriography showed retrograde filling of the celiac axis via a prominent pancreaticoduodenal arcade (Figure 3). Given the tortuosity and pushability required to select the subsegmental hepatic artery supplying the tumor in segment 8 via the SMA, a triaxial system was utilized. The triaxial system consisted of a 5-F, 45-cm Ansel sheath (Cook Medical), a 5-F Cobra 2 Glidecath (Terumo Interventional Systems), and a Renegade STC microcatheter (Boston Scientific Corporation) (Figure 4). A corresponding angiogram (Figure 5) and cone-beam CT (Figure 6) confirmed tumor vascularity supplied via the selected segment 7 branch.

A 3.7% lung shunt was calculated following technetium-99m macroaggregated albumin injection. Using partition dosimetry and a target tumor dose of 200 Gy, an injected activity of 30 mCi (1.1 GBq) was calculated for the segmental infusion. One week after mapping, Y-90 administration was performed via the retrograde SMA approach, with resin microspheres delivered to the segment 7 branch. Immediate posttreatment single-photon emission CT (SPECT)-CT images demonstrated marked tumoral uptake (Figure 7). Follow-up MRI examinations

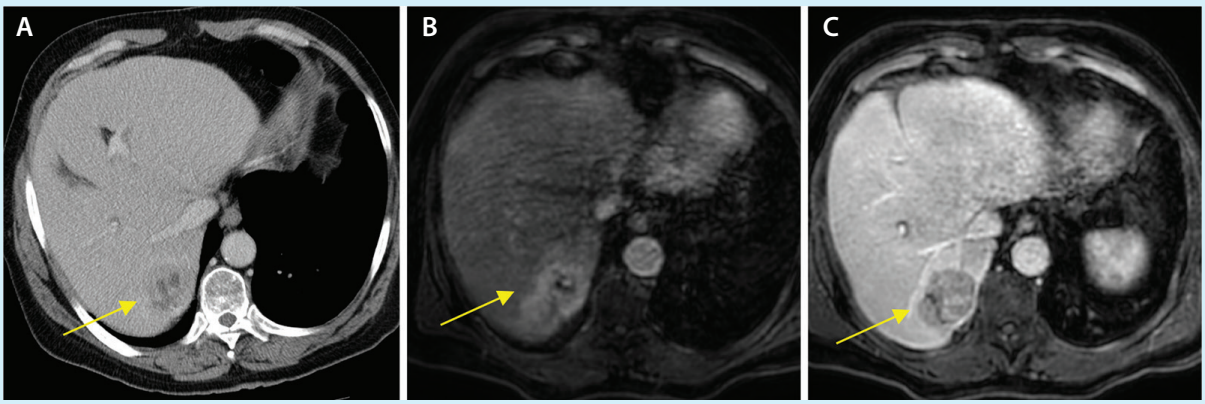

Figure 1. Contrast-enhanced CT (A) and MRI images show a segment 7 mass (arrows) with arterial enhancement (B) and venous washout (C).

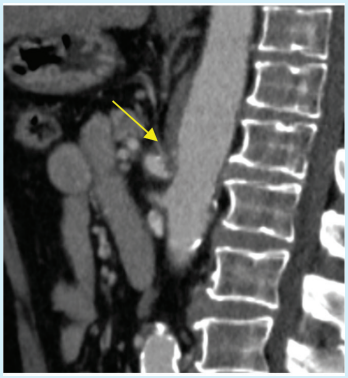

Figure 2. Celiac occlusion (arrow) secondary to diaphragmatic compression and atherosclerotic disease, shown on sagittal contrast-enhanced CT.

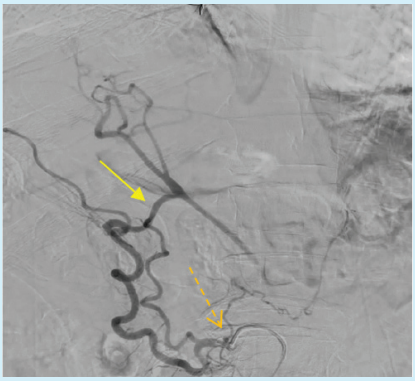

Figure 3. An arteriogram with a 5-F catheter in the pancreaticoduodenal artery (dotted arrow) via the SMA shows retrograde filling of the celiac axis and hepatic arteries via the prominent pancreaticoduodenal arcade and gastroduodenal artery (arrow).

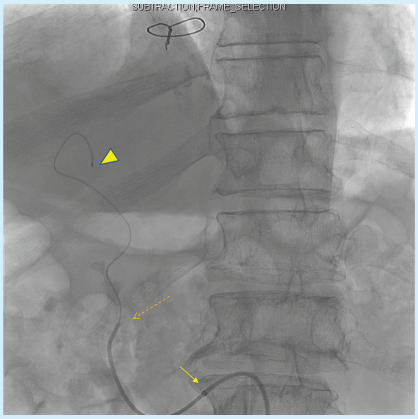

Figure 4. Retrograde hepatic arterial catheterization and angiography via the SMA using a 5-F, 45-cm Ansel sheath (arrow), a 5-F Cobra 2 Glidecath (dashed arrow), and a Renegade STC microcatheter (arrowhead).

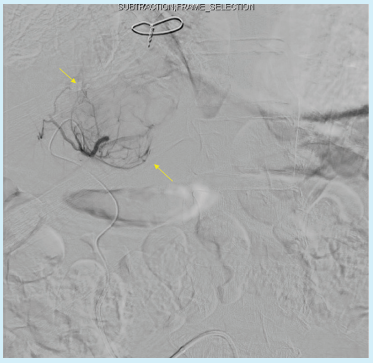

Figure 5. Retrograde hepatic catheterization shows tumor vascularity (arrow) supplied by the segment 7 branch.

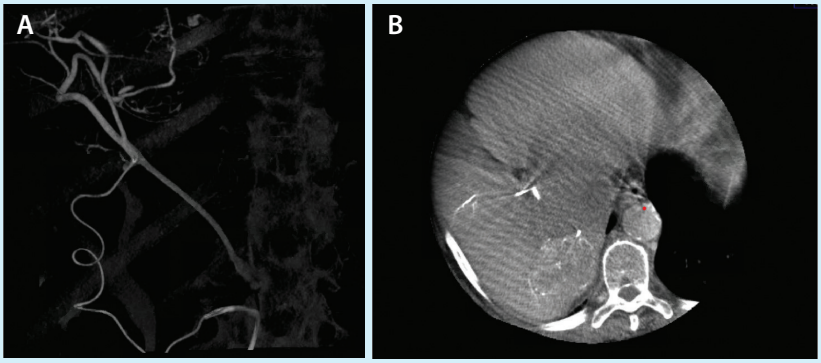

Figure 6. Cone-beam CT axial reconstruction shows the tumor vascularity (A), and three-dimensional reconstruction shows the tortuosity of the approach to the treatment vessel (B).

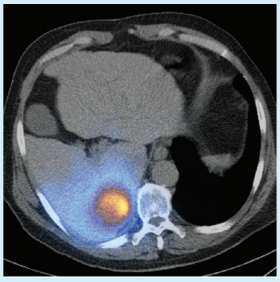

Figure 7. Post–Y-90 SPECT-CT confirmed segmental and tumor uptake after radiation segmentectomy.

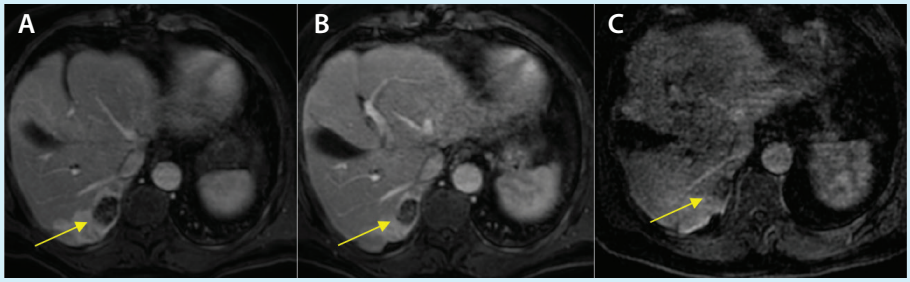

Figure 8. Portal venous-phase, contrast-enhanced MRI taken at 6 (A), 9 (B), and 15 months (C) postprocedure showed lack of tumor enhancement, progressively decreased lesion size, and surrounding segmental atrophy (arrows), consistent with expected changes after radiation segmentectomy.

have shown a progressively decreased size of the treated lesion, without evidence of residual or recurrent disease (Figure 8).

DISCUSSION

Radioembolization has shown good results in patients with early stage HCC who are not candidates for resection, transplantation, or thermal ablation. Radiation segmentectomy allows targeted delivery of ablative radiation doses while minimizing nontarget parenchymal toxicity; response rates for solitary, unresectable tumors after radiation segmentectomy are comparable to other curative-intent treatments.[1,2]

Celiac occlusion may be encountered during transarterial locoregional therapies and is frequently secondary to diaphragmatic compression. When the occlusion cannot be traversed, a retrograde SMA approach may be used to catheterize the proper hepatic artery via pancreaticoduodenal arcades and the gastroduodenal artery.[3,4] When retrograde approaches fail, transsplenic and transhepatic access have also been described for radioembolization in the setting of celiac occlusion.[5,6]

1. Salem R, Johnson GE, Kim E, et al. Yttrium-90 radioembolization for the treatment of solitary, unresectable HCC: the LEGACY study. Hepatology. 2021;74:2342-2352. doi: 10.1002/hep.31819
2. Arndt L, Villalobos A, Wagstaff W, et al. Evaluation of medium-term efficacy of Y90 radiation segmentectomy vs percutaneous microwave ablation in patients with solitary surgically unresectable hepatocellular carcinoma: a propensity score matched study. Cardiovasc Intervent Radiol. 2021;44:401-413. doi: 10.1007/s00270-020-02712-1
3. Attia NM, Othman MHM. Transcatheter arterial chemoembolization of hepatocellular carcinoma in patients with celiac axis occlusion using pancreaticoduodenal arcade as a challenging alternative route. Eur J Radiol Open. 2017;4:53-57. doi: 10.1016/j.ejro.2017.04.002
4. Moraes AO, do Nascimento EA, Zubiolo TFM, et al. Transcatheter arterial chemoembolization of hepatocellular carcinoma in a patient with celiac trunk occlusion: a therapeutic challenge. J Vasc Bras. 2019;18:e20180090. doi: 10.1590/1677-5449.180090
5. Hsu MJ, Tran DN, Srinivasa RN, et al. Transsplenic arterial radioembolization of hepatic metastases in a patient with celiac artery occlusion. J Vasc Interv Radiol. 2019;30:1604-1605. doi: 10.1016/j.jvir.2018.12.024
6. Yu M, Lewandowski RJ, Ibrahim S, et al. Direct hepatic artery puncture for transarterial therapy in liver cancer. J Vasc Interv Radiol. 2010;21:394-399. doi: 10.1016/j.jvir.2009.11.003

Mohammad Bader, MD
Division of Interventional Radiology
Boston Medical Center
Assistant Professor of Radiology
Boston University School of Medicine
Boston, Massachusetts
mohammad.bader@bmc.org
Disclosures: None.

Suvranu Ganguli, MD, FSIR
Division of Interventional Radiology
Boston Medical Center
Professor of Radiology
Boston University School of Medicine
Boston, Massachusetts
suvranu.ganguli@bmc.org
Disclosures: Consultant to Sirtex, Boston Scientific Corporation, Medtronic, Instylla, ABK Medical, Avania/Boston Biomedical Associates.

Complete Response of Oligometastatic Renal Cell Carcinoma After Combined Hepatic Embolization and Ablation

By Paraag R. Gupta, BS, and Amy R. Deipolyi, MD, PhD, FSIR

The National Comprehensive Cancer Network (NCCN) recommends metastasectomy or ablative techniques with complete resection of disease for stage IV or relapsed renal cell carcinoma (RCC)[1] because large retrospective studies suggest prolonged survival and periods free of systemic therapy when metastatic disease can be eradicated.[2] Metastasectomy may entail surgical resection, external radiation, or thermal ablation. Because no prospective studies compare relative efficacy of these locoregional therapies, the choice of modality depends on the patient's functional status and comorbidities and the size and location of the tumors.

CASE PRESENTATION

A man in his 80s with a history of papillary type 2 RCC with lymphovascular invasion and renal vein involvement with 6 of 12 lymph nodes positive for metastatic carcinoma was referred for management of an enlarging liver lesion. He had undergone an open left nephrectomy with negative margins. Within 1 year, he developed a left hepatic lesion, which was biopsied and demonstrated metastatic RCC, and a painful lytic L1 metastasis with pathologic fracture. He underwent external radiation to the vertebral metastasis and was referred for consideration of liver-directed therapy. The tumor was fluorodeoxyglucose (FDG)-avid on positron emission tomography (PET)/CT (Figure 1A) and measured > 4 cm, with an irregular contour evident on ultrasound (Figure 1B and 1C). Given the large size and configuration of the hepatic tumor, he was offered combined bland hepatic embolization with microwave ablation (MWA).

PROCEDURAL OVERVIEW

The procedure was performed under general anesthesia in a supine position. Angiography demonstrated a large hypervascular tumor in the left hepatic lobe supplied by the left hepatic artery, which was replaced to the left gastric artery (Figure 2A). The segment 2/3 artery was embolized using 40–120-µm Embospheres (Merit Medical) and 300-µm polyvinyl alcohol particles until complete stasis. Under ultrasound and cone-beam CT guidance, MWA was performed using a 15-cm PR XT

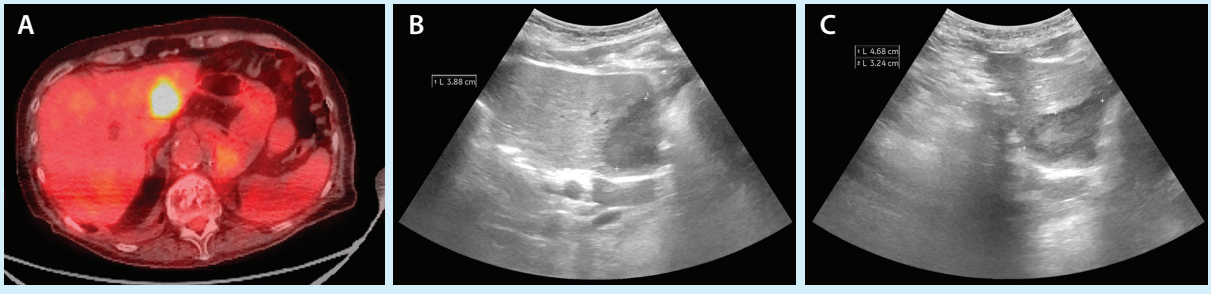

Figure 1. Preprocedural imaging. PET/CT demonstrates an FDG-avid tumor in segment 2/3 measuring > 4 cm (A). Transabdominal ultrasound in sagittal (B) and transverse (C) views demonstrate that the tumor had an irregular contour with an oblong, lobulated configuration and measured nearly 5 cm in the longest axis.

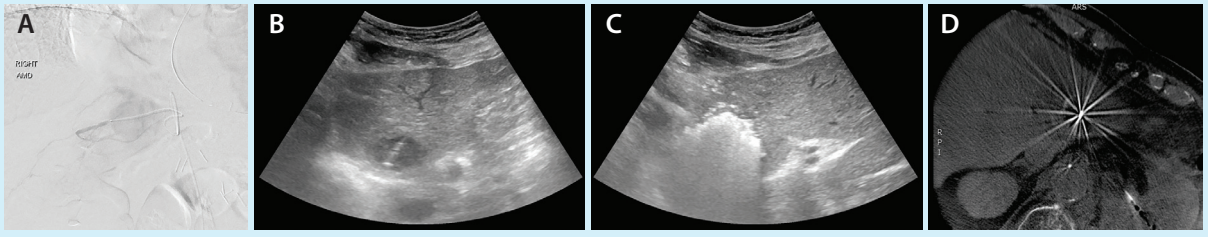

Figure 2. Combined hepatic bland embolization and thermal ablation. Angiography demonstrates a hypervascular tumor in the left lobe supplied by the left hepatic artery and replaced to the left gastric artery (A). Intraprocedural ultrasound demonstrates the probe within a portion of the tumor (B) and echogenic foci during the thermal ablation (C). Intraprocedural cone-beam CT demonstrates the ablation probe centered within the hyperdense embolized tumor (D).

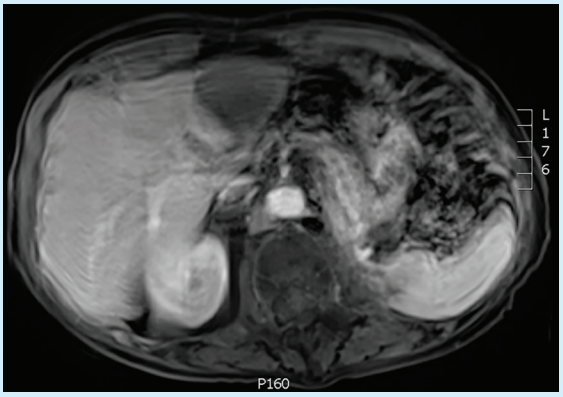

Figure 3. MRI performed 6 weeks later demonstrates a wide zone of ablation, with no residual disease or new lesions.

NeuWave applicator (Ethicon, a subsidiary of Johnson & Johnson) at four positions at 65 W for a total of 9 minutes (Figure 2B-2D). The patient tolerated the procedure well, with expected postembolization/ablation syndrome symptoms. Follow-up contrast-enhanced MRI 6 weeks later demonstrated complete response, with no residual or new lesions (Figure 3).

DISCUSSION

Compared with surgical resection and external radiation, liver-directed therapy with embolization or thermal ablation can provide complete response with minimal hospitalization or outpatient visits. Thermal ablation is typically preferred for smaller lesions. Because it is more difficult to achieve adequate margins when ablating large tumors, such ablations are associated with higher rates of residual disease.[3] For tumors > 3 cm, combining embolization with thermal ablation is one approach to increase the ablation zone size, thereby improving the margins and outcomes. Performing embolization immediately before thermal ablation prevents vascular collateralization and reperfusion, maximally boosting the size of the ablation zone.[4] Furthermore, it reduces the number of invasive procedures the patient must undergo for oncologic control.

Most data published regarding combined embolization/ablation for liver tumors have described its use in the treatment of HCC. Both HCC and RCC demonstrate avid arterial enhancement,[5] suggesting that particulate embolics will preferentially deposit in RCC metastases, as seen in HCC. Given that the NCCN recommends locoregional therapies with an intent for tumor eradication, achieving the largest-possible ablation zone for RCC liver metastases may entail combination strategies used in treating HCC. Combining bland embolization with thermal ablation is one such strategy that can be considered in similar cases.

1. National Comprehensive Cancer Network. Kidney cancer. Version 2.2023. 2023 Accessed August 26, 2022. https://www.nccn.org/professionals/physician_gls/pdf/kidney.pdf
2. Ouzaid I, Capitanio U, Staehler M, et al. Surgical metastasectomy in renal cell carcinoma: a systematic review. Eur Urol Oncol. 2019;2:141-149. doi: 10.1016/j.euo.2018.08.028
3. Shiina S, Tateishi R, Arano T, et al. Radiofrequency ablation for hepatocellular carcinoma: 10-year outcome and prognostic factors. Am J Gastroenterol. 2012;107:569-577. doi: 10.1038/ajg.2011.425
4. Gennaro N, Poretti D, Ferrillo G, et al. Single-session bland embolisation followed by microwave ablation for hepatocellular carcinoma: chasing anatomic resection. Cardiovasc Intervent Radiol. 2021;44:336-338. doi: 10.1007/s00270-020-02695-z
5. Akın IB, Altay C, Güler E, et al. Discrimination of oncocytoma and chromophobe renal cell carcinoma using MRI. Diagn Interv Radiol. 2019;25:5-13. doi: 10.5152/dir.2018.18013

Paraag R. Gupta, BS
MD Candidate
West Virginia University School of Medicine
Morgantown, West Virginia
prgupta@mix.wvu.edu
Disclosures: None.

Amy R. Deipolyi, MD, PhD, FSIR
Associate Professor of Surgery
Director of Interventional Radiology
WVU Charleston Division/Charleston Area Medical Center
Charleston, West Virginia
amy.deipolyi@camc.org
Disclosures: None.

Palliative Biliary Stenting for Recurrent Ampullary Carcinoma

By Christopher R. Bailey, MD, and Kelvin Hong, MD

CASE PRESENTATION

A man in his early 70s with a history of ampullary adenocarcinoma treated with a robotic-assisted Whipple procedure 2 years prior presented with fevers, chills, and dark urine. Of note, the patient had completed adjuvant chemotherapy but was found to have recurrent disease during active surveillance. Initial emergency department diagnostic evaluation was significant for a total bilirubin level of 10.9 mg/dL and a CT demonstrating new intrahepatic biliary ductal dila-

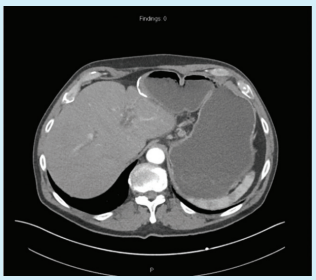

Figure 1. Contrast-enhanced CT of the abdomen demonstrates right and left intrahepatic biliary ductal dilation.

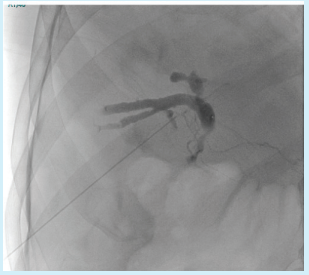

Figure 2. Initial PTC demonstrates moderate intrahepatic biliary ductal dilation with high-grade HJ stricture. Access was obtained using a 22-gauge Chiba needle (Cook Medical).

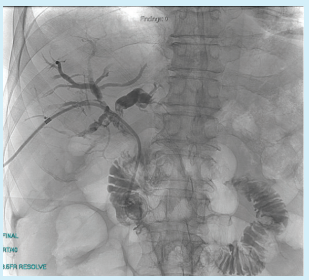

Figure 3. Postplacement cholangiography through the 8.5-F PBD catheter.

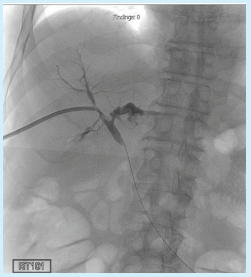

Figure 4. The initial over-the-wire cholangiogram after removal of initial PBD demonstrates improved intrahepatic biliary ductal dilation, with stable high-grade HJ stricture.

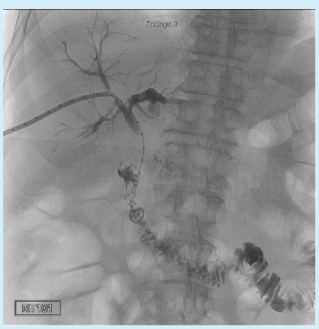

Figure 5. The cholangiogram with 5-F marker pigtail catheter in place to measure the required stent length.

Figure 6. A postdeployment cholangiogram of the 10-mm X 6-cm Viabil self-expanding covered stent across the stricture demonstrates delayed flow of contrast across the stricture with persistent intrahepatic ductal dilation.

Figure 7. Postdeployment cholangioplasty of the Viabil stent with the 8-mm X 4-cm Conquest balloon.

Figure 8. The final postprocedural cholangiogram, with brisk clearance of contrast through the Viabil stent and improved intrahepatic biliary ductal dilation.

tion (Figure 1). Given his known recurrence and new hyperbilirubinemia and fevers, the patient was started on broad-spectrum antibiotics for cholangitis, and interventional radiology (IR) was urgently consulted for percutaneous biliary decompression given the post-Whipple procedure bilioenteric anatomy.

PROCEDURAL OVERVIEW

The initial percutaneous transhepatic cholangiogram (PTC) demonstrated moderate intrahepatic biliary ductal dilation with a high-grade stricture at the hepaticojejunostomy (HJ) compatible with tumor recurrence (Figure 2). The stricture was successfully crossed using an Accustick introducer system (Boston Scientific Corporation), 4-F angle-taper Glidecath, and a 0.035-inch Glidewire (Terumo Interventional Systems), and an 8.5-F ReSolve internal-external biliary drain (Merit Medical Systems, Inc.) was placed, yielding purulent bile (Figure 3). The patient was left to external drainage for 48 hours; his fevers/chills resolved, and the purulent bile cleared. Total bilirubin improved slightly to 9.0 mg/dL. Given the patient's known recurrence,

estimated life expectancy of under 1 year, and remote living situation that limited his ability to travel for routine tube exchanges and upsizes, the decision was made to convert the internal-external biliary drainage catheter to an internal biliary stent.

The patient was brought back to the IR suite for conversion to the internal biliary stent after 72 hours of biliary decompression with the 8.5-F tube. The internal-external biliary tube was exchanged for a 10-F sheath over an Amplatz wire. Initial over-the-wire cholangiography demonstrated internal improvement in biliary ductal dilation with a persistent high-grade HJ stricture (Figure 4). A 5-F marker pigtail catheter was placed over the Amplatz wire into the small bowel and pulled back to the HJ while injecting contrast to determine the length of stent required. The distance from the proximal common bile duct to the HJ was 5 cm; thus, the decision was made to place a 10-mm X 6-cm Viabil self-expanding covered stent (Gore & Associates). The marker pigtail catheter and sheath were removed over the Amplatz wire, and the Viabil stent introducer sheath was advanced into position and deployed across the HJ stricture (Figure 5). A postdeployment cholangiogram demonstrated slow clearance of contrast across the HJ stricture (Figure 6). The decision was made to perform cholangioplasty of the stricture with an 8-mm X 4-cm Conquest balloon (BD Interventional) (Figure 7). The final cholangiogram demonstrated significant improvement in the HJ stricture, with brisk clearance of contrast and improved decompression of the intrahepatic biliary tree (Figure 8). The wires and sheaths were removed with no external tube left in place. Postprocedure, the patient did well with no further episodes of cholangitis and improvement of total bilirubin to 7.1 mg/dL at 48 hours after biliary stenting. He was discharged to home with no further episodes of cholangitis.

DISCUSSION

Approximately 70% to 90% of biliary obstructions occur secondary to advanced malignancy (pancreatic adenocarcinoma, cholangiocarcinoma, ampullary/duodenal carcinoma, gallbladder cancer, and metastatic disease).[1] However, this is often the presenting symptom of primary or recurrent disease because most of these malignancies remain asymptomatic until later stages. Common presentations include jaundice, pruritus, and dark urine. Prolonged biliary stasis can lead to severe cholangitis. Management of malignant biliary strictures requires discussion and planning from a multidisciplinary team of surgeons, medical oncologists, gastroenterologists, and interventional radiologists.

Both endoscopic and interventional techniques can be used for diagnostic and therapeutic evaluation of biliary strictures. Endoscopic retrograde cholangiopancreatography (ERCP) is usually first line for diagnostic and therapeutic evaluation because it uses natural orifice for access and can provide direct internal drainage. In patients with surgically altered anatomy, such as this case patient, ERCP can be technically challenging or impossible. Complications from ERCP include pancreatitis, hemobilia, and cholangitis. In cases of altered surgical anatomy, PTC with placement of a percutaneous biliary drain (PBD) is usually pursued, but there is a higher risk profile (bleeding/hemobilia, damage to surrounding structures) because this technique requires the creation of a parenchymal tract in the liver. There is also an increased risk of cholangitis after PTC/PBD due to transpapillary reflux of gastrointestinal bacteria and subsequent catheter dysfunction/blockage.[1]

Although PTC/PBD is a well-tolerated procedure with a high success rate, its major long-term drawback is external catheter discomfort and required catheter maintenance to prevent occlusion. In patients with unresectable or recurrent malignancy, internal biliary stenting with self-expanding metallic stents (SEMSs) can be deployed to prevent the need for a percutaneous drain. SEMSs can be deployed through both endoscopic and percutaneous approaches, as in our case. Compared to plastic stents, SEMSs have significantly greater patency times (approximately 6-9 months) but eventually become occluded with tumor ingrowth/progression. To combat tumor ingrowth, covered SEMSs were developed. Multiple randomized studies have demonstrated lower rates of stent occlusion and increased primary patency with covered SEMSs[2,3]; however, more recent studies have conflicted the earlier body of evidence, suggesting that there is no significant difference between covered and uncovered SEMSs regarding patency, occlusion rates, and overall survival.[4] In a recent meta-analysis evaluating randomized controlled trials spanning 21 studies with 2,326 patients who received uncovered or covered SEMSs for malignant extrahepatic biliary obstruction, tumor ingrowth was common in the uncovered SEMSs group, while stent migration, tumor overgrowth, and occlusion by sludge were common in the covered SEMSs group.[5] However, the overall risk of recurrent biliary obstruction did not differ between uncovered versus covered internal biliary stents. This highlights the recent controversy/discrepancy in the literature regarding stent choice (covered vs metallic alone). However, internal metallic stents have superior efficacy regarding recurrent obstruction compared to plastic stents, as well as

quality-of-life benefits compared with internal-external biliary drains.

In summary, internal biliary stenting from a percutaneous approach can give patients with surgically altered anatomy a durable solution for their malignant biliary obstruction, without negatively impacting quality of life.

1. Bailey CR, Hong K. Obstructive jaundice. In: Digestive Disease Interventions. Thieme Medical Publishers; 2018.
2. Krokidis M, Fanelli F, Orgera G, et al. Percutaneous treatment of malignant jaundice due to extrahepatic cholangiocarcinoma: covered Viabil stent versus uncovered Wallstents. Cardiovasc Intervent Radiol. 2010;33:97-106. doi: 10.1007/s00270-009-9604-9
3. Krokidis M, Fanelli F, Orgera G, et al. Percutaneous palliation of pancreatic head cancer: randomized comparison of ePTFE/FEP-covered versus uncovered nitinol biliary stents. Cardiovasc Intervent Radiol. 2011;34:352-361. doi: 10.1007/s00270-010-9880-4
4. Dhondt E, Vanlangenhove P, De Man M, et al. No advantage of expanded polytetrafluoroethylene and fluorinated ethylene propylene-covered stents over uncovered nitinol stents for percutaneous palliation of malignant infrahilar biliary obstruction: results of a single-center prospective randomized trial. J Vasc Interv Radiol. 2020;31:82-92. doi: 10.1016/j.jvir.2019.07.013
5. Park CH, Park SW, Jung JH, et al. Comparative efficacy of various stents for palliation in patients with malignant extrahepatic biliary obstruction: a systematic review and network meta-analysis. J Pers Med. 2021;11:86. doi: 10.3390/jpm11020086

Christopher R. Bailey, MD
Vascular and Interventional Radiology
Russell H. Morgan Department of Radiology and Radiological Science
Johns Hopkins Hospital
Baltimore, Maryland
Disclosures: None.

Kelvin Hong, MD
Vascular and Interventional Radiology
Russell H. Morgan Department of Radiology and Radiological Science
Johns Hopkins Hospital
Baltimore, Maryland
khong1@jhmi.edu
Disclosures: None.

Intraprocedural Nerve Monitoring During Cryoablation for Pain

By Raul N. Uppot, MD, FSIR, FSAR, and Reiner Henson B. See, MD

CASE PRESENTATION

A woman in her late 50s with endometrial cancer metastasis to the left pelvis presented with debilitating left pelvic pain. She described 10 out of 10 pain localized to the left pelvic region and radiating to the proximal upper thigh. She was referred to IR for pain management. On diagnostic CT, there was a mass near the left femoral, obturator, and sciatic nerves (Figure 1). In the IR clinic, plans were made for CT-guided ablation to debulk the mass. Cryoablation was chosen due to its known history for tumor debulking for pain control and the ability to closely monitor its approximation to nearby nerves by observing the edge of the ice ball.

PROCEDURAL OVERVIEW

Based on imaging, the cryoablation area would be critically close to nerve tissue. The challenge of this case was that the proximity of the mass to these nerves risked loss of motor function, including a permanent left foot drop. A neurology consultation was obtained to consider intraprocedural nerve monitoring.

Neurology recommended the use of free-run electromyography (EMG) neurophysiologic monitoring to detect early and reversible neurophysiologic dysfunction that may arise from inadvertent thermal injury to nearby neural tissue. Spontaneous free-run EMG discharges could be generated in peripheral nerves from compression, traction, laceration, or thermal irritation.

The patient underwent CT-guided cryoablation under general anesthesia. Upon sedation of the patient by the anesthesia team, the neuromonitoring team placed needle EMG electrodes on muscles of the left leg. The specific muscles were innervated by nerves in the proximity of the cryoablation ball and were at risk of thermal injury. Free-run EMG monitoring required avoiding use of any neuromuscular blockade or paralytic agent. General endotracheal anesthesia was required to maintain a quiet surface EMG baseline and avoid false-negative signals due to patient motion.

The patient was turned to the right lateral decubitus position. As each cryoablation probe was placed, continuous real-time surface EMGs were obtained for any evidence of nerve irritation to ensure that none of the probes physically transgressed the nerves or branches of the nerves during cryoprobe insertion. There was no spontaneous EMG activity noted during probe placement.

Once all probes were satisfactorily positioned within the tumor, cryoablation was started (Figure 2). Typically, we perform a cycle of 10-minute freeze, 8-minute passive thaw, and 10-minute freeze, with CT images obtained at 0, 3, 6, and 10 minutes and again at 3, 6, and 10 minutes in the second freeze cycle. However, in cases where there is concern for potential injury to critical structures in close proximity, we obtain images every 2 minutes and thus proceeded in this manner for this case.

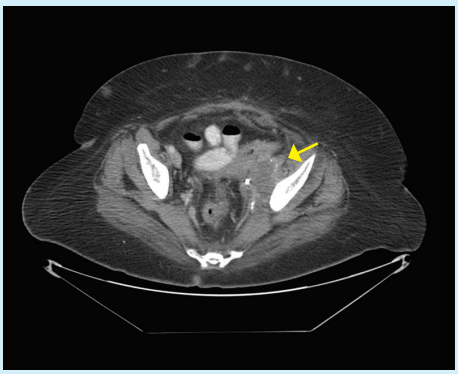

Figure 1. Axial CT showing left pelvic mass (arrow). The mass abuts courses of the left femoral, sciatic, and obturator nerve.

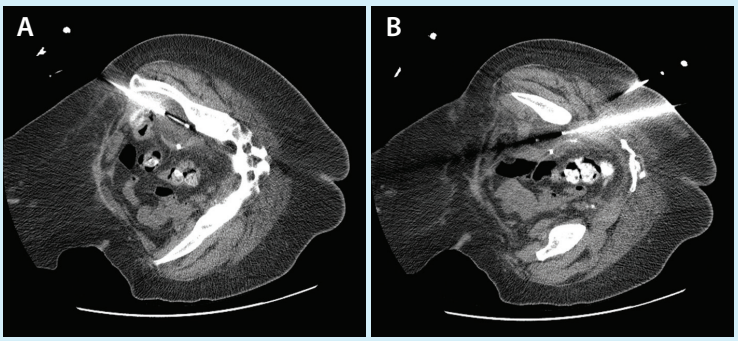

Figure 2. CT-guided cryoablation under anesthesia. The patient was in the right lateral decubitus position, and multiple cryoablation probes were placed. The anterior cryoprobe with the ice ball visualized (A). Posterior cryoprobes with the ice ball visualized (B).

Within 60 seconds of activating the cryoprobe to expand the ice ball, there was a gradual increase of EMG activity observed only from the left tibialis anterior muscle (Figure 3). This was characterized initially by a small polyspike EMG discharge with a small amplitude of 20-40 µV and a frequency of < 1 Hz. The EMG discharges progressed and evolved to higher amplitudes of > 1,400 µV and frequency of 2 to 3 Hz. The left tibialis anterior muscle is innervated by the deep peroneal nerve, which is a distal branch of the sciatic nerve (Figure 3). The cryoablation machine was immediately turned off. However, there was a persistent increase in surface EMG activity, and the decision was made to initiate the active thaw process on the cryoablation machine to rapidly melt the ice ball. The reported EMG activity from the left tibialis anterior muscle immediately returned to a baseline state of quiet EMG activity.

The procedure was carefully continued with the remaining other probes that were far from the left sciatic nerve to further debulk the tumor. No further nerve irritation activity was noted, and the probes were removed.

Postprocedure, the patient had improvement in pain from a 10/10 to 0/10. However, she did have numbness along the inner thigh and a left foot drop. In the hospital, she had slight improvement and was discharged to rehabilitation where she had further improvement. She passed away 6 weeks after the procedure due to progression of metastatic disease.

CASE SUMMARY

This palliative care patient had improvement in pain and avoided permanent sciatic nerve injury due to intraprocedural nerve monitoring. The sciatic nerve was likely irritated by cryoablation; however, because intraprocedural nerve monitoring detected sciatic nerve irritation within 60 seconds of the cryoablation probe being turned on and the issue was addressed by active thaw, permanent nerve injury was avoided. Had we waited until the first CT scan as planned at 2 minutes, more of the ice ball would have encompassed the sciatic nerve for a longer time, likely resulting in colder exposure and permanent nerve injury.

DISCUSSION

Image-guided cryoablation has gained a foothold in the management of intractable pain.[1-3] Cryoablation achieves pain control by freezing small sensory nerves at the tumor/soft tissue interface or by direct destruction of sensory nerves. Although cryoablation is now used to treat pain that has failed other options (including narcotics, surgery, radiation, and chemotherapy), the challenge in image-guided cryoablation is to selectively target the sensory/pain fibers while minimizing damage to adjacent neural tissue within proximity of the thermal ablation zone. Although visualization of the ice ball edge helps finely define the location of tissue destruction, optical viewing of the ice ball is not adequate to define motor versus sensory nerve destruction. An effective adjunct to preventing morbidity in complex cryoablation procedures is the use of neurophysiologic monitoring. Intraoperative neurophysiologic monitoring, or neuromonitoring, is proven effective and has been the standard of care in high-risk neurosurgical and orthopedic procedures for decades.[4-6]

Neuromonitoring uses cutting-edge multimodality neurophysiologic techniques to warn when neural tissue is at risk of injury during the procedure.[7] A few published series have detailed the use of nerve moni-

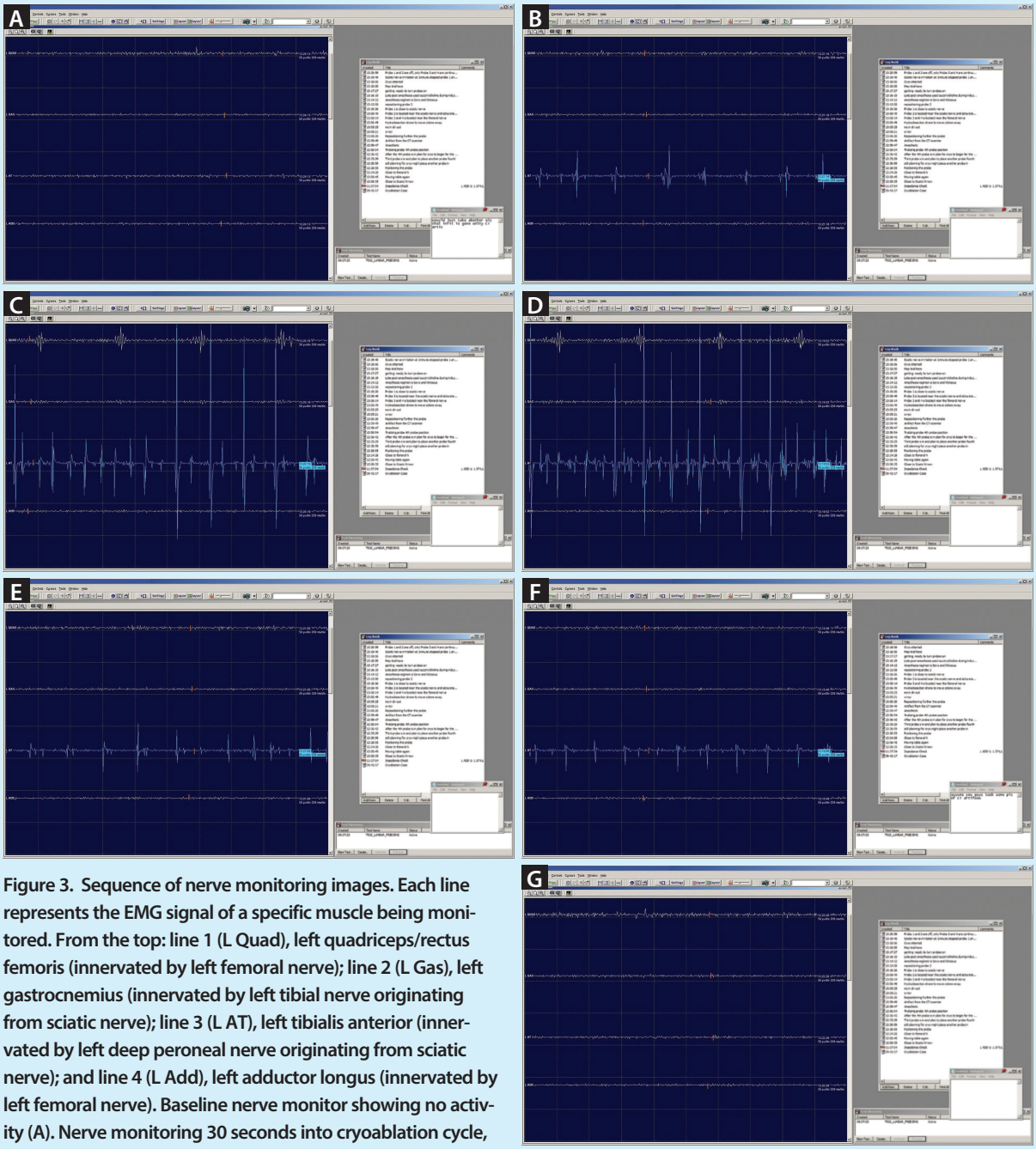

Figure 3. Sequence of nerve monitoring images. Each line represents the EMG signal of a specific muscle being monitored. From the top: line 1 (L Quad), left quadriceps/rectus femoris (innervated by left femoral nerve); line 2 (L Gas), left gastrocnemius (innervated by left tibial nerve originating from sciatic nerve); line 3 (L AT), left tibialis anterior (innervated by left deep peroneal nerve originating from sciatic nerve); and line 4 (L Add), left adductor longus (innervated by left femoral nerve). Baseline nerve monitor showing no activity (A). Nerve monitoring 30 seconds into cryoablation cycle, again showing no activity (B). Nerve monitoring 60 seconds into cryoablation cycle showing activity in the sciatic nerve (C). Nerve monitoring 62 seconds into the cryoablation cycle showing increased activity in the sciatic nerve (D). Nerve monitoring after cryoablation probe was turned off showing persistent increased activity in the sciatic nerve (E). Nerve monitoring 1 second after active thaw was turned on showing decreased activity in the sciatic nerve (F). Nerve monitoring after 5 seconds of active thaw showing return of sciatic nerve activity to baseline (G). Panel D adapted from See RB, Dineen J, Winograd J, Simon M. Intraoperative neurophysiology in peripheral nerve surgery. In: Simon M, editor. Intraoperative Neurophysiology: A Comprehensive Guide to Monitoring and Mapping. Demos Medical Publishing; 2018:539-577.

toring during cryoablation.[8,9] Prior to the procedure, a detailed knowledge and understanding of the surrounding neuroanatomy is key to preventing iatrogenic nerve injury. A detailed preprocedural discussion between the interventional radiologist and the neurologist is necessary to review the available radiographic images, discuss the planned approach for the tumor or trajectory of the thermal ablation probe, and, most importantly, determine the relevant neuroanatomic structures that are at risk for injury within the thermal ablation zone.

The radiologist determines neural structures that are at risk for injury, and the neurologist tailors a neuromonitoring plan that includes a neurophysiologic modality technique to monitor each specific neural tissue at risk. The neuroanatomic structures adjacent to the ablation zone should be outlined, and neurophysiologic modalities appropriate for monitoring those structures should be chosen. Real-time nerve monitoring offers physiologic monitoring of nerve function and is often used by neurosurgeons and orthopedic surgeons intraoperatively to carefully dissect tissue and avoid permanent nerve injury. The types of nerve monitoring range from simple detection of muscle fasciculations as a proxy for defined nerve activity to active transcranial stimulation for detecting function of specific nerves.

Cryoablation works in conjunction with nerve monitoring due to differential degrees of nerve injury based on exposure to different temperatures. Seddon[10] and Sunderland[11] developed a classification of nerve injury from cryotherapy:

- Class I: Neuropraxia that occurs when the nerve is exposed to temperatures from +10° to −20° C. The endoneurium, perineurium, and epineurium are intact, and there is no Wallerian degeneration. With class I injury, the nerve function recovers within days to weeks.
- Class II: Axonotmesis that occurs when the nerve is exposed to temperatures from −20° to −100° C. There is injury to the axon and endoneurium, and there is Wallerian degeneration. Recovery from class II injury takes months.
- Class III: Neurotmesis that occurs when the nerve is exposed to temperatures < 140° C. There is injury to the axon and surrounding connective tissue, and there is Wallerian degeneration. Class III injury is likely permanent and can only potentially be addressed with nerve grafting.

Nerve monitoring helps because the early physiologic activity detected is likely from the periphery of the ice ball with warmer temperatures. Less cold temperatures lead to recovery of nerve function. In a study of 59 procedures to treat 64 tumors in 52 patients, use of nerve monitoring showed that the risk of major motor injury with persistent motor evoked potential (MEP) changes was significantly increased versus transient or no MEP change (relative risk, 69.8; 95% CI, 5.9 to > 100; $P = .0045$).[9] In another more recent retrospective review of 29 patients (16 male; median age, 46 years; range, 7-77 years), abnormal activity during nerve monitoring correlated with postprocedural neurologic sequelae.[8]

This case demonstrates that use of intraprocedural nerve monitoring during ablation can selectively destroy tumor and sensory nerve fibers (for pain control) while minimizing permanent motor nerve injury. Incorporation of such tools can expand the scope of tumors that can be ablated by interventional radiologists. ■

1. Ramadhyani S. Cryoablation for the treatment of solid cancers and pain management. In: Shrivastava D, editor. Theory and Applications of Heat Transfer in Humans. Wiley: 2018:687-714.
2. Ferrer-Mileo L, Blanco AIL, González-Barboteo J. Efficacy of cryoablation to control cancer pain: a systematic review. Pain Pract. 2018;18:1083-1098. doi: 10.1111/papr.12707
3. Hitt E. Cryoablation provides pain relief. Lancet Oncol. 200;9;8:15. doi: 10.1016/s1470-2045(07)70400-x
4. Murena L, Colin G, Dussi M, Canton G. Is intraoperative neuromonitoring effective in hip and pelvis orthopedic and trauma surgery? A systematic review. J Orthop Traumatol. 2021;22: 40. doi: 10.1186/s10195-021-00605-8
5. Zheng C, Song J, Liu S, et al. Intraoperative electromyographic techniques for the decision-making of tumor-involved nerve root resection for treating spinal schwannomas. Spine J. 2021;21:1900-1907. doi: 10.1016/j.spinee.2021.05.013
6. Salzman SK. Neural Monitoring: The Prevention of Intraoperative Injury. Springer Science & Business Media; 2012.
7. See RB, Dineen J, Winograd J, Simon M. Intraoperative neurophysiology in peripheral nerve surgery. In: Simon M, editor. Intraoperative Neurophysiology: A Comprehensive Guide to Monitoring and Mapping. Demos Medical Publishing; 2018:539-577.
8. Yoon JT, Nesbitt J, Raynor BL, et al. Utility of motor and somatosensory evoked potentials for neural thermoprotection in ablations of musculoskeletal tumors. J Vasc Interv Radiol. 2020;31:903-911. doi: 10.1016/j.jvir.2019.12.015
9. Kurup AN, Morris JM, Boon AJ, et al. Motor evoked potential monitoring during cryoablation of musculoskeletal tumors. J Vasc Interv Radiol. 2014;25:1657-1664. doi: 10.1016/j.jvir.2014.08.006
10. Seddon HJ. A classification of nerve injuries. Br Med J. 1942;2:237-239. doi: 10.1136/bmj.2.4260.237
11. Sunderland S. A classification of peripheral nerve injuries producing loss of function. Brain. 1951;74:491-516. doi: 10.1093/brain/74.4.491

Raul N. Uppot, MD, FSIR, FSAR
Division of Interventional Radiology
Massachusetts General Hospital
Associate Professor
Harvard Medical School
Boston, Massachusetts
uppot.raul@mgh.harvard.edu
Disclosures: Consultant to Boston Scientific Corporation.

Reiner Henson B. See, MD
Neurologist
Intraoperative Neurophysiology Unit
Department of Neurology
Massachusetts General Hospital
Clinical Instructor of Neurology
Harvard Medical School
Boston, Massachusetts
rsee@mgh.harvard.edu
@reinersee
Disclosures: None.